



PCCP

**Core Structure Dependence of Cycloreversion Dynamics in
Diarylethene Analogs**

Journal:	<i>Physical Chemistry Chemical Physics</i>
Manuscript ID	CP-ART-10-2019-005797.R1
Article Type:	Paper
Date Submitted by the Author:	09-Jan-2020
Complete List of Authors:	Honick, Chana; Johns Hopkins University, Chemistry Peters, Garvin; Johns Hopkins University, Chemistry Young, Jamie; Johns Hopkins University, Chemistry Tovar, John; Johns Hopkins University, Chemistry Bragg, Arthur; Johns Hopkins University, Chemistry

SCHOLARONE™
Manuscripts

Core Structure Dependence of Cycloreversion Dynamics in Diarylethene Analogs

Chana R. Honick, Garvin M. Peters, Jamie D. Young, John D. Tovar, and Arthur E. Bragg*
Department of Chemistry, Johns Hopkins University
3400 N. Charles St., Baltimore, MD 21218
**artbragg@jhu.edu*

Abstract: Diarylperfluorocyclopentenes are a well-characterized class of molecular photoswitches that undergoes reversible photocyclization. The efficiency of cycloreversion (<~30%), in particular, is known to be limited by a competition with excited-state deactivation by internal conversion that is strongly impacted by the electron-withdrawing/donating character of pendant aryl groups. Here we present a first study to determine how varied structural motifs for the core bridge group impact excited-state dynamics that control cycloreversion quantum yields. Specifically, we compare photophysical behaviors of 3,3'-(perfluorocyclopent-1-ene-1,2-diyl)bis(2-methylbenzo[*b*]thiophene) with diarylethene derivatives possessing the same benzo[*b*]thiophene pendant group but with a rigid 1-methyl-1*H*-pyrrole-2,5-dione and a

rigid/aromatic thieno[3,4-*b*]thiophenbridge (TT) core bridge group. We find that the flexible perfluorocyclopentene core undergoes cycloreversion 3-4x slower than the rigid core photoswitches (9 vs. 2-3 ps in acetonitrile, 25 vs. 5-6 ps in cyclohexane) despite comparable cycloreversion quantum yields. To distinguish effects induced by bridge vs pendant groups, we also studied a series of photoswitches with the same thieno[3,4-*b*]thiophene bridging group, but with varied pendant groups including 2,5-dimethylthiophene and 2-(3,5-bis(trifluoromethyl)phenyl)-5-methylthiophene. Analysis of temperature-dependent excited-state lifetimes and cycloreversion quantum yields reveals that both the rates of nonreactive internal conversion and reactive cycloreversion increase with greater structural rigidity of the core. This difference is attributed to smaller energy barriers on the excited-state potential energy surface for both reactive and non-reactive deactivation from the 2^1A electronic state relative to the flexible perfluorocyclopentene switch, implying that a rigid core results in a net shallower excited-state potential energy surface.

Introduction: Molecular photoswitching is possible when a molecule undergoes reversible isomerization between two or more structures following isomer-selective absorption of light. Photoswitches can be used to manipulate both optical and electronic material properties and have been investigated widely for optoelectronic applications including optical memory storage and optical gating of molecular electronics.¹⁻⁷ For precision performance, it is imperative that photoswitches have high thermal stability, rapid response times, high switching efficiency (i.e. quantum yield), and fatigue resistance over many switching cycles.^{1, 2, 8-14} Activation with visible to near infrared wavelength light is particularly advantageous for utilizing widely available and inexpensive light sources (e.g. LEDs), as well as for improving penetration depths through

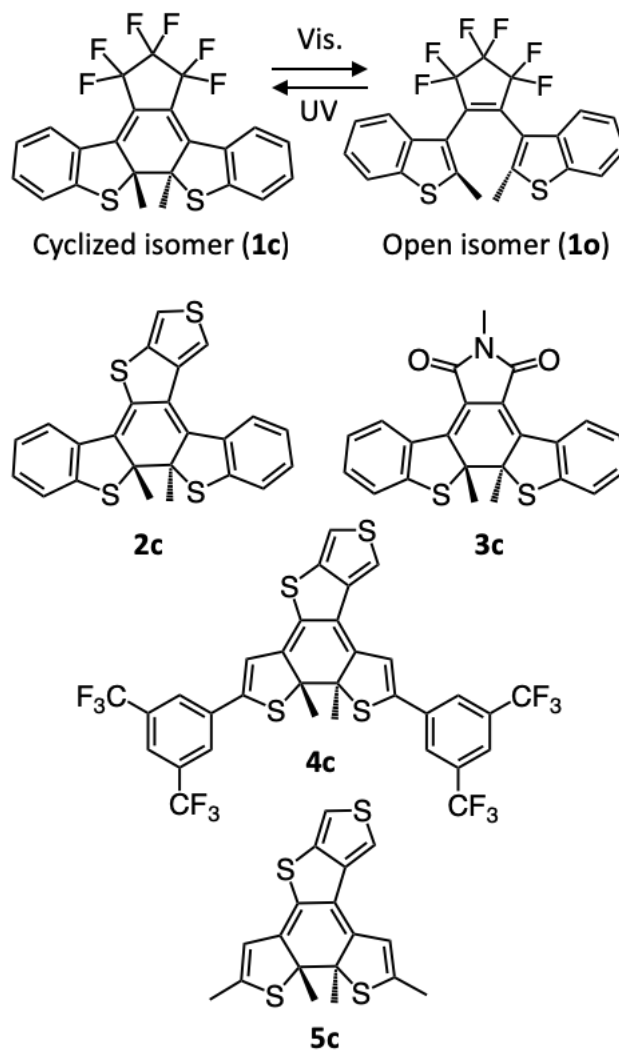
materials and biological tissue.¹ Diarylethenes (DAE) are a class of photoswitch that possess many of these desirable characteristics.^{1, 2, 10} For example, bis(benzo[b]thienyl)perfluorocyclopentene (**1o**), shown in Scheme 1, undergoes electrocyclization following excitation of its lowest-energy absorption while cycloreversion follows after selective visible excitation of the lowest absorption of its cyclized isomer (**1c**). Notably, specific absorption characteristics of the open and closed isomers depend on the structure (e.g. extent of conjugation across the cyclized isomer). Some DAE derivatives have been shown to undergo rapid reversible cyclization several thousand times, and in the absence of light, many can remain in one form or another indefinitely.^{15, 16}

There has been extensive synthetic exploration of this class of compounds in recent years with demonstrated improvements in isomerization quantum yields and fatigue resistance via structural modifications to the pendant groups that form a bond during the cyclization.^{9, 10, 17-21} This work has been accompanied by a number of computational²²⁻²⁶ and ultrafast spectroscopic investigations²⁷⁻³⁵ to address how these modifications alter the shapes of and dynamics on excited-state potential energy landscapes that underlie their switching efficiencies. For DAEs like **1o**, the origins of inefficiencies depend on switching direction. Photocyclization efficiency is generally limited in solution by thermal population of both reactive parallel and non-reactive antiparallel conformers^{2, 26}, whereas switching efficiency can be significantly higher in crystals that favor the reactive conformer as a result of molecular packing.^{13, 31, 36-38} Cyclization is also inefficient for structures with large initial separations between the reactive carbon sites of the pendant rings.¹⁷ Thus, DAEs in a crystal with a C-C separation $<4 \text{ \AA}$ exhibit cyclization quantum yields approaching unity.

On the other hand, cycloreversion yields are comparatively lower for normal-type DAE switches, usually much less than 0.5.²² The prevailing rationale for this behavior is that a

significant energetic barrier exists on the 2^1A excited-state surface that separates nonreactive and reactive conical intersections (CIs) for deactivation (i.e. “internal conversion” vs. “cycloreversion”); this barrier is nominally associated with avoided crossings with higher-lying states of the same (A) symmetry.^{22, 25} Temperature-dependent interrogation of cycloreversion quantum yields and ultrafast excited-state deactivation dynamics in **1c**, in particular, provided empirical support for this excited-state barrier,³² while computations reveal that the magnitude of this barrier, which dictates accessibility of the reactive CI for ring opening, is strongly dependent on the properties of pendant groups.²² Under these circumstances, increasing the efficiency of ring opening requires tuning or manipulating ultrafast dynamics on excited-state potential energy surfaces to favor transit to a CI for cycloreversion. Recent strategies towards the improvement of switching performance involve multi-photon induced and temperature-dependent photoswitching,^{29, 30, 32, 39-42} both of which require additional external stimuli. A more general strategy for improving switch performance is to differentiate the structure-dynamics relationships associated with these two processes to control their relative rates in favor of cycloreversion.

Scheme 1. Photoconversion between the cyclized (**1c**) and open (**1o**) isomers of 3,3'-(perfluorocyclopent-1-ene-1,2-diyl)bis(2-methylbenzo[*b*]thiophene), and structures of the closed isomers (**c**) of photoswitches investigated in this work: 3,3'-(thieno[3,4-*b*]thiophene-2,3-diyl)bis(2-methylbenzo[*b*]thiophene) (**2o/2c**), 1-methyl-3,4-bis(2-methylbenzo[*b*]thiophen-3-yl)-1*H*-pyrrole-2,5-dione (**3o/3c**), 2,3-bis(5-(3,5-bis(trifluoromethyl)phenyl)-2-methylthiophen-3-yl)thieno[3,4-*b*]thiophene (**4o/4c**), and 2,3-bis(2,5-dimethylthiophen-3-yl)thieno[3,4-*b*]thiophene (**5o/5c**).



Notably, prior efforts focused on the properties of switches that share a common core/bridge motif, perfluorocyclopentene (e.g., **1o** in Scheme 1). Indeed, perfluorocyclopentene has been the most commonly studied DAE bridging group to date due to its stability and non-reactivity. Ultrafast dynamics of cyclization and cycloreversion have been studied almost exclusively with switches built from this bridging group, including photoswitches with various pendent groups: 1,2-bis(2,4-dimethyl-5-phenyl-3-thienyl),^{29, 30} 1,2-bis(2-methyl-5-(2-(4-benzoyl-phenyl-vinyl))-thien-3-yl),⁴³ 1,2-bis(5-formyl-2-methyl-thien-3-yl),^{33, 44} bis(2-methyl-5-phenylthiophen-3-yl),^{39-41, 45} and 1,2-bis(2-methylbenzo[*b*]-thiophen-3-yl)^{32, 46, 47}. All of these

switches have qualitatively similar cycloreversion dynamics in hexane or cyclohexane with initial spectral relaxation occurring on timescales ranging 1-4 ps that is attributed to fast structural evolution in the excited state, and with subsequent excited-state lifetimes ranging from 9 to 25 ps. These relatively long excited-state lifetimes may enable deactivation pathways competitive with cycloreversion.

Although perfluorocyclopentene-core switches have demonstrated considerable success, other switch cores could exhibit useful function. For example, aromatic bridging groups have been considered synthetically for purposes of linking switchable chromophores to larger conjugated structures to enable photo-switchable electronic properties. We recently integrated a thienothiophene core (e.g. as in **2**) into DAEs to facilitate synthesis of core-linked oligomers with electronic properties controllable through the cyclization of peripheral groups.⁴⁸ It could be hypothesized that photoinduced cycloreversion may be favored with the introduction of core aromaticity due to an anticipated increase in the stability of the open isomer relative to a structure with a less globally aromatic core: e.g., in the case of **2**, one would expect a difference in stability between the 6π aromatic system in the closed form and the 10π aromatic system in the open form. Irie and coworkers have also shown that introducing an aromatic thiophene bridging group alters the pi-conjugation of both the open and closed-form isomers.⁴ Steady-state properties of these systems were altered as a result of extending conjugation through the bridging group, but the impact of an aromatic rigid core group on switching dynamics and efficiency has not been examined explicitly. A related study on excited-state topologies of dihydroazulene-photoswitches indicated that changes in aromaticity along the potential energy surface could significantly alter switching characteristics, particularly hampering switching when the excited transition-state involves a loss in aromaticity.⁴⁹

Notably, ultrafast switching dynamics may also be strongly affected by the inherent rigidity of the core bridging group: this rigidity could significantly impact the potential energy landscape and barriers for structural relaxation to critical excited-state geometries (i.e. conical intersections) for nonadiabatic cycloreversion, thereby reducing the rate and efficiency of cycloreversion relative to other deactivation processes. Alternatively, a rigid core could be expected to constrain or funnel excited-state dynamics to critical structures, resulting in faster switching dynamics.⁵⁰ This second possibility is notable because the standard perfluorocyclopentene core structure is comparatively flexible, which could facilitate structural evolution along excited-state potential-energy surfaces to local excited-state minima resulting in somewhat longer excited-state lifetimes.

In order to address the role of core bridge structure on photoswitch properties, we present an investigation of the ultrafast cycloreversion dynamics and quantum yields for a series of photoswitches **1c-3c** (Scheme 1) that contain various core/bridge motifs including perfluorinated cyclopentene (**1c**), a rigid, aromatic thieno[3,4-*b*]thiophene (**2c**), and a rigid non-aromatic 1-methyl-1*H*-pyrrole-2,5-dione (**3c**), but all with common benzo[*b*]thiophene pendant groups. We also present the analysis of a series of photoswitches with a common thienothiophene core motif but with various pendant groups (**2c**, **4c** and **5c**). By comparing photophysics of these five compounds, we extend current understanding of excited-state dynamics in DAE photoswitches and particularly the impact of core structure on the shape of the excited-state potential energy surface that control these dynamics and cycloreversion quantum yields.

2. Experimental methods.

2.1 Sample Preparation and Handling. 3,3'-(perfluorocyclopent-1-ene-1,2-diyl)bis(2-methylbenzo[*b*]thiophene) (**1o**) (> 97.0 %) was purchased from TCI America and used as

received. 3,3'-(thieno[3,4-*b*]thiophene-2,3-diyl)bis(2-methylbenzo[*b*]thiophene) (**2o**), 1-methyl-3,4-bis(2-methylbenzo[*b*]thiophen-3-yl)-1*H*-pyrrole-2,5-dione (**3o**),⁵¹ 2,3-bis(5-(3,5-bis(trifluoromethyl)phenyl)-2-methylthiophen-3-yl)thieno[3,4-*b*]thiophene (**4o**),⁴⁸ and 2,3-bis(2,5-dimethylthiophen-3-yl)thieno[3,4-*b*]thiophene (**5o**),⁴⁸ were synthesized and purified as described elsewhere; the synthetic details for **2** are described in the Supporting Information. Sample solutions were prepared by dissolving **1o**, **2o**, **3o**, and **4o** both in acetonitrile and in cyclohexane at concentrations ranging from $\sim 0.6\text{--}20 \times 10^{-3}$ M. A solution of **5o** was only prepared in acetonitrile at similar concentrations. Each sample was subsequently converted to a photostationary state of open- and cyclized isomers through prolonged irradiation at 320 nm with an ultraviolet hand lamp resulting in concentrations of the cyclized form at steady state ranging $\sim 1\text{--}4 \times 10^{-4}$ M. We include a spectrum of the hand lamp in the Supporting Information Figure S28. Photostationary solutions were stored in the dark following preparation to inhibit photoinduced cycloreversion.

Steady-state UV-Vis spectra of photoconverted samples were collected both before and after time-resolved measurements using a diode-array spectrometer with fiber-optically coupled tungsten and deuterium lamps (Stellarnet). To prevent a significant drop in concentration of the cyclized isomer throughout the course of time-resolved measurements, each solution was continuously pumped through a flow cell (variable pathlength from Harrick Scientific Products or a 1mm quartz flowcell from Spectrocell) from a solution reservoir contained in a quartz round-bottom flask. The quartz flask was irradiated with a UV hand lamp throughout the course of each measurement to maintain a photostationary state. The optical path-length of the flow cell was either 0.5 mm, 0.95 mm, or 1 mm depending on the optical density of the closed isomer at excitation wavelengths used for ultrafast measurements. Optical densities in the flow cell ranged from ~ 0.03

to 0.3. A cryostat with a 1 cm cuvette was used for temperature-dependent transient absorption and quantum yield measurements. Temperature-dependent ultrafast measurements were conducted over a short acquisition timescale (~1 min.) and samples were stirred rapidly in order to minimize sample loss due to photoconversion. A reference signal collected periodically at a fixed pump-probe time delay was also collected in order to normalize transient signals with respect to conversion as a result of irradiation of sample cuvettes with ultrafast pulses.

2.2 Transient Absorption Spectroscopy. A regeneratively amplified Ti:sapphire laser system (Coherent Legend Elite, 1 kHz rep. rate, 35 fs pulse duration, 4.0 mJ/pulse) was used to generate laser pulses for ultrafast spectroscopic measurements. Pump pulses centered at 500 nm, 530 nm, and 600 nm were generated with an optical parametric amplifier (OPA, Coherent Operasolo) via signal+800 nm sum-frequency generation with fluences ranging from ~28 to ~250 $\mu\text{J}/\text{cm}^2$; no power dependence of dynamics were observed in this range. These wavelengths are selectively resonant with the lowest energy 500 nm absorption features of **1c**, **2c**, and **3c**, the 600 nm absorption feature of **4c**, and the 530 nm absorption feature of **5c** (vide infra), ensuring the absence of contaminating spectral signals in transient spectra that would be associated with photoinduced cyclization of the open isomers. A broadband probe continuum (~380-700 nm) was generated by focusing 800 nm ultrafast pulses through a calcium fluoride (CaF_2) plate. A temporal window of 10-1200 ps was achieved by retro-reflecting the pump beam off of a hollow corner cube mirror mounted onto a motorized translation stage (Newport). To remove the effects of polarization anisotropy, the probe beam was directed through a wire-grid polarizer set to magic angle relative to the pump beam polarization. After passing through the sample, the probe beam was filtered to remove features below 370 nm and above 800 nm and was dispersed and focused onto a

multichannel array. Probe spectra were collected and transient absorption subsequently calculated shot-to-shot with a homebuilt LabVIEW program described elsewhere.^{52, 53} Our time resolution (pump-probe cross-correlation) was approximately 120 fs for these measurements. However, large-amplitude coherent artifacts contributed significantly to signals measured within a few hundred femtoseconds of time zero. Time-resolved spectra collected at time delays from 0.5 ps and beyond were used in global fitting analyses, as we could not differentiate faster spectral dynamics from coherent signals at shorter delays.

2.3 Molar Absorptivity and Quantum Yield Determinations.

The molar absorptivities of **1o-5o** were determined from a Beer's Law analysis of steady-state UV-Vis absorption measurements with solutions at various photoswitch concentrations in a 1-mm cuvette. The molar absorptivities for **1c-5c** in relation to **1o-5o** were determined using chromatographic separations of photostationary mixtures of the isomers in combination with UV-Vis absorption spectroscopy. Chromatographic separations used reverse-phase HPLC (methanol/water eluent with a 00D-4725-AN Kinetex® column from Phenomenex, particle size: 2.6 μm , pore size: 100 Å, length: 100 mm for **1o/c**, **2o/c**, **3o/c**, **4o/c**, and 200 mm for **5o/c**). The fraction of closed isomer within the photostationary mixture was determined based on the fractional drop in the open-isomer concentration measured before and after irradiation to the photostationary state. The relative absorptivities of the two isomers were determined at a fixed wavelength in the UV by normalizing the absorption spectra measured for each isomer after HPLC separation by the fraction of each isomer recovered; the absolute extinction coefficient for the closed isomer could then be determined relative to that of the open isomer. Details pertaining to

the determination of molar absorptivities (including a list of determined values) are provided in Section 2 of the Supporting Information.

The cycloreversion quantum yields of each system were determined using photochemical actinometry.^{54, 55} We used the cycloreversion of 1,2-bis(2,4-dimethyl-5-phenyl-3-thienyl)-3,3,4,4,5,5-hexafluoro-1-cyclopentene (98.0% TCI) as an actinometric standard because the quantum yields had been determined previously at several excitation wavelengths in the range of 480-620 nm.¹⁴ This standard was used specifically to determine the photon flux of a 496 nm (cyan, FWHM: 485-507nm) light emitting diode (LED) (Led World via Amazon, ASIN: B00MO9O7Q8) used to drive isomerization of **1c**, **2c**, **3c**, and **5c** as well as a 596 nm (yellow FWHM:587-602nm) LED (Sparkfun: Model No.: YSL-R1031Y2C-D14) used to drive isomerization of **4c**. These LEDs were chosen to match the maxima of the ground state absorption of the closed structures and also because they do not overlap with absorption features of open isomers. Temperature-dependent quantum yields for cycloreversion of **1c-3c** were determined using a cryostat (Unisoku) by the same general method. For these measurements, the quantum yield of each switch at 298 K was used as a standard in order to determine the photon flux through the cryostat. The absorption spectra of closed switches (without LED irradiation) were also measured at various temperatures to account for any changes in molar absorptivity with temperature when determining quantum yields. Full experimental details for acquiring and analyzing data for quantum-yield determinations are described further in the Supporting Information.

3. Results.

3.1 Steady-state spectroscopic characterization.

The molar absorptivities ($M^{-1}cm^{-1}$) of **1-5** as both open and closed isomers are plotted in Figure 1 (a-e); steps for determining these values are outlined in the Supporting Information (see, e.g. Figures S1-S6). The absorption spectra of **1o** and **1c** are similar to those published previously.^{32, 46, 47} The absorption onset for **2o**, **4o** and **5o** are similar to that of **1o**, whereas the lowest-energy absorption of **3o** is shifted noticeably to a longer wavelength. The lowest-energy absorption features of **1c**, **2c**, **3c**, and **5c** fall near 500 nm, with differences in the positions of higher energy features. In contrast, the lowest-energy absorption of **4c** falls to longer wavelength (~600 nm). These spectral changes from open to closed structures are consistent with breaking aromaticity of the open structure via cyclization to create delocalized polyene network. These spectra also illustrate that quantum yield and ultrafast transient measurements conducted with light sources at 500 nm and longer wavelengths should be selective for excitation of the closed isomer.

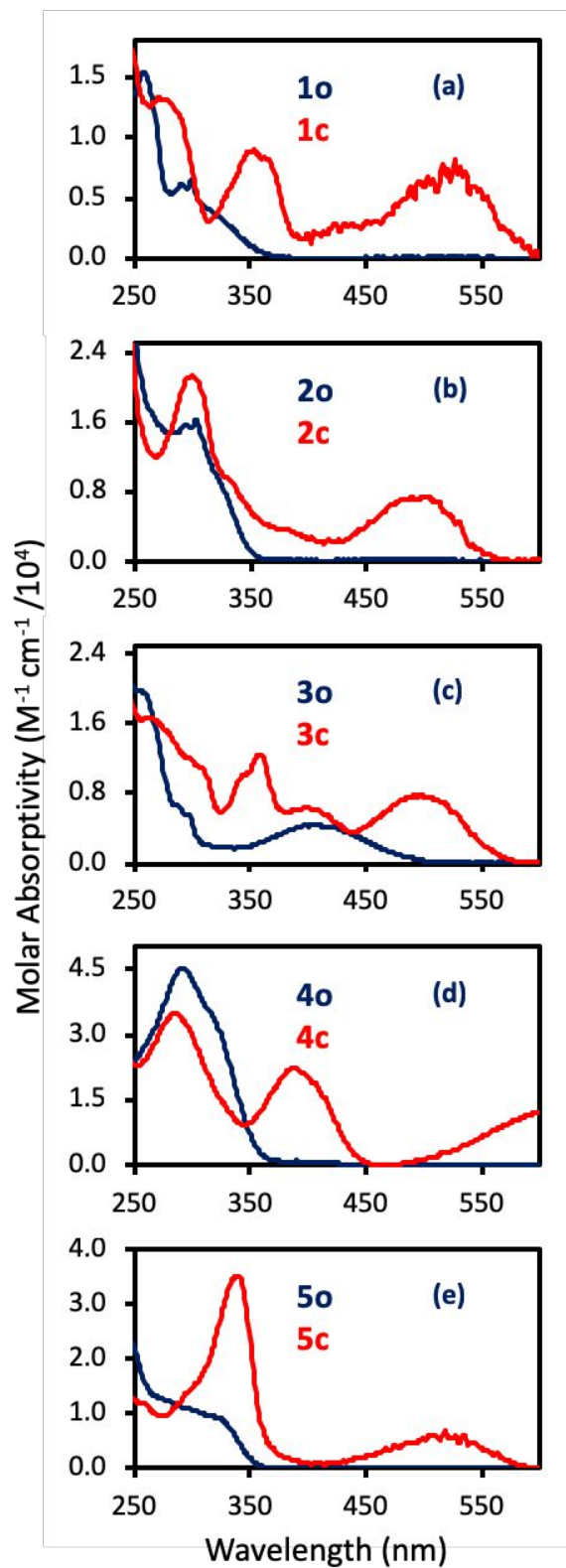


Figure 1. Molar absorptivities for the open and closed isomers of **1-5** in acetonitrile.

3.2 Ultrafast characterization of excited-state dynamics.

3.2.1 Core-dependence of excited-state dynamics (**1c-3c**).

Figures 2a, 2b, and 2c display transient absorption spectra collected following 500 nm excitation of **1c-3c** in acetonitrile as probed across the visible. For **1c**, transient spectra closely resemble those reported by Shim et al., but with some differences in spectral evolution arising from differences in solvent environment that will be discussed further below. Here we observe a narrow absorption feature centered about 695 nm as well as a few weaker features at 634, 555, and 435 nm that overlap with the region of the lowest-energy steady-state absorption feature for **1c**. All absorption features decay within 100 ps; notably, a bleach of the ground-state absorption spectrum (“ground-state bleach,” or GSB) with peak near 530 nm appears at latest delays examined, consistent with the partial depletion of **1c** through cycloreversion to **1o**.

The transient spectra for **2c** and **3c** are somewhat different: At 0.5 ps, **2c** exhibits a slight negative intensity at 515 nm with photoinduced absorption both at shorter and longer wavelengths. As the lowest-energy feature in the ground-state absorption spectrum peaks roughly in the middle of this region, we interpret spectra at earliest delays to reflect a combination of both GSB and photoinduced absorption. Similar to **2c**, **3c** exhibits a broad absorptive feature extending across the visible spectrum, with the GSB overlapping the absorption at 502 nm that blueshifts slightly to 498 nm on a sub-picosecond timescale. Like **1c**, **3c** also exhibits an intense photoinduced absorption above 700 nm. **3c** also exhibits a signature of a stimulated emission (SE) band at 665 nm that overlaps its excited-state absorption features. By the latest delays probed the photoinduced absorption (and emission) features have decayed and GSB appears near 500 nm, likewise indicating conversion of **2c** and **3c** to **2o** and **3o**, respectively. Contrary to **1c**, **2c** and **3c** both

exhibit a minor bleach recovery that is associated with the decay of an absorption just to the red of the bleach; for reasons described below, we attribute this to relaxation of a vibrationally hot ground electronic state.

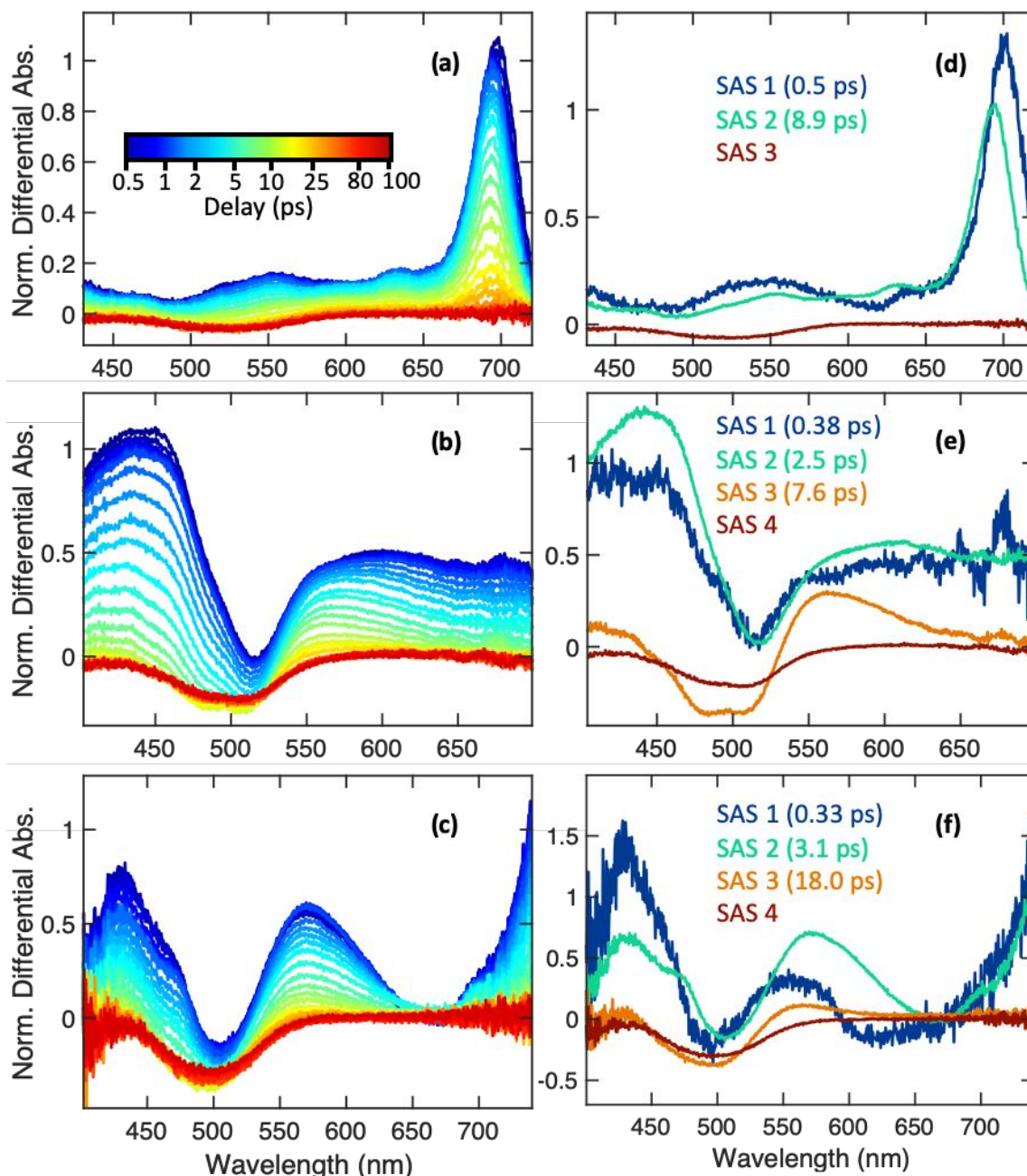


Figure 2. Transient absorption spectra collected for **1c** (a), **2c** (b), and **3c** (c) in acetonitrile at selected time delays ranging from 0.5ps to 100ps as well as the corresponding species-associated spectra (SAS) as determined through global fitting for **1c** (d), **2c** (e), and **3c** (f). Data was normalized to 1 at maximum absorption at 1ps.

Figure 2d, 2e, and 2f plot the species associated spectra (SAS) obtained through principal component global analysis of TA data for **1c-3c** subject to series, state-to-state kinetic models for all transient data collected after a delay of 0.5 ps. Figure 3 plots the time-dependent global fits for transients of different probe wavelengths across the visible (450 nm; 550 nm; 630 nm; and 700 nm) for each switch; spectral reconstructions from global fits and residuals are presented in Figures S7-S9. Best-fit lifetimes obtained for each switch are summarized in Table 1. Transient data collected for **1c** was fit with a three-state series model, yielding interconversion lifetimes of 0.5 ps and 8.9 ps. The shorter lifetime is associated with a rapid spectral shifting/relaxation of the initial excited state (τ_{relax}) whereas the slower timescale is associated with the overall excited-state lifetime ($\tau_{decay 1}$).

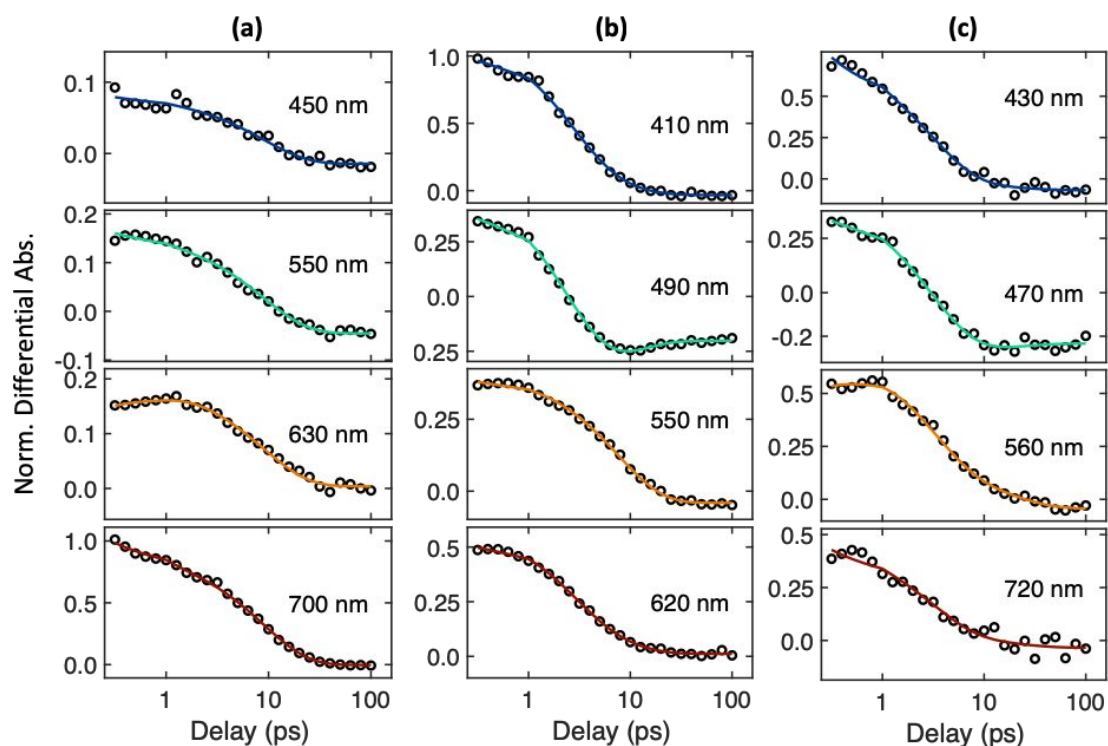


Figure 3. Time-dependent global fits for **1c** (column a), **2c** (column b), and **3c** (column c) in acetonitrile. Data after 0.5 ps is plotted on a linear scale <1 ps and on a logarithmic scale >1 ps to clarify early time spectral dynamics.

Table 1. Summary of fit parameters obtained by global analysis of TA measurements for **1c**, **2c**, and **3c** in acetonitrile and cyclohexane.

	Acetonitrile				Cyclohexane			
	τ_{relax} (ps)	$\tau_{decay 1}$ (ps)	$\tau_{decay 2}$ (ps)	$\tau_{vib.}$ (ps)	τ_{relax} (ps)	$\tau_{decay 1}$ (ps)	$\tau_{decay 2}$ (ps)	$\tau_{vib.}$ (ps)
1c	0.5	8.9	-	-	0.48	4.6	25.7	-
2c	0.38	2.5	-	7.6	0.57	5.3	-	10.6
3c	0.33	3.1	-	18.0	-	1.4	6.2	13.9

In contrast, global fitting of data collected for **2c** and **3c** required a four-state series kinetic model. Global fits yield state interconversion timescales of 0.38 ps, 2.5 ps, and 7.6 ps for **2c** and 0.33 ps and 3.1 ps, and 18 ps for **3c**. As for **1c**, we attribute the shortest timescale with relaxation within the excited state(s), while the intermediate timescale is associated with excited-state decay. Notably, there is a significant decrease in excited-state lifetime between **1c** and **2c-3c**. As indicated above, we assign the longest timescale obtained for **2c** and **3c** with decay of a vibrationally hot state ($\tau_{vib.}$) of the fraction of the switch population that relaxes back to the electronic ground state without opening. Our assignment of this longer timescale to vibrational relaxation is supported by the shape of SAS3: there is extra absorption to the red of the GSB (550 nm), where we expect absorption of a vibrationally hot switch in its ground state to appear, but lacks significant absorption appearing above 600 nm and below 500 nm that appear in SAS1 and SAS2 and is attributable to excited-state absorption. It is interesting that a clear signature of a vibrationally hot ground state is not captured for **1c**, which likely reflects that vibrational cooling occurs on a timescale that is comparable to or faster than electronic deactivation of **1c**.

3.2.2 Solvent dependence of excited-state dynamics (1c-3c).

Prior ultrafast investigations of cycloreversion dynamics were conducted in various solvents, and we therefore used both acetonitrile and cyclohexane to facilitate comparisons with reports in the literature.⁴⁷ Ultrafast transient spectra, as well as results from global fits for transient data collected with **1c-3c** in cyclohexane are reported in the Supporting Information (Figure S10-S15). Fit parameters are summarized in Table 1. **1c** exhibits pronounced differences in spectral dynamics in cyclohexane vs. acetonitrile. Notably, there is an overall shift in the major absorption feature at ~698 towards ~710 nm. Global fitting of spectral dynamics for **1c** in cyclohexane requires a four-component sequential model and reveals an additional lifetime associated with absorption decay. The global fit yielded a short lifetime of 0.48 ps (τ_{relax}) associated with early time spectral evolution (i.e. shifts), as well as 4.6 (τ_{decay1}) and 25.7 ps (τ_{decay2}) lifetimes associated with evolution in the intensity of excited-state absorption features. These results are in close agreement with the results reported by Shim et al., who reported results for **1c** in n-hexane including a major absorption feature at 710 nm and excited-state lifetimes of 4 and 22 ps.⁴⁶

Like **1c**, **2c** and **3c** both show a ~10 nm shift in spectral features towards lower energy from acetonitrile to cyclohexane. However, **2c** does not exhibit an additional excited-state signal decay lifetime in cyclohexane while **3c** does: **2c** excited-state signal decay is slowed in cyclohexane from 2.5 to 5.3 ps, while the excited state signal decay for **3c** in cyclohexane is slowed from a single 3.1 ps timescale to a bimodal decay with lifetimes of 1.4 and 6.2 ps. Vibrational cooling of ground-state **2c** and **3c** after excited-state deactivation is observable in both solvents. In summary, all three switches exhibit a dilation by a factor of ~2.1-2.8 of the excited-state lifetimes in cyclohexane vs. acetonitrile, suggesting that the impact of solvent environment on deactivation dynamics is comparable regardless of the core structure. Curiously, the bimodal decays for **1c** and **3c** in cyclohexane reflect changes in the timescales of nuclear dynamics on the excited-state potential

energy surface in cyclohexane; these are discussed further below in context of previous interpretations of ultrafast spectral dynamics collected with similar systems.

3.2.3 Temperature-dependent excited-state lifetimes (**1c-3c**).

Temperature-dependent TA measurements focused on the variation in the excited-state lifetime of each switch dissolved in acetonitrile. These lifetimes are plotted in Figure 4; examples of corrected transient data are presented in Figure S16. Noticeably, the excited-state lifetime of **1c** is consistently much longer than those of **2c** and **3c** at all temperatures, while the excited-state lifetime of **3c** is only slightly longer than that of **2c**. Further analysis of these data in combination with temperature-dependent quantum yields are presented below.

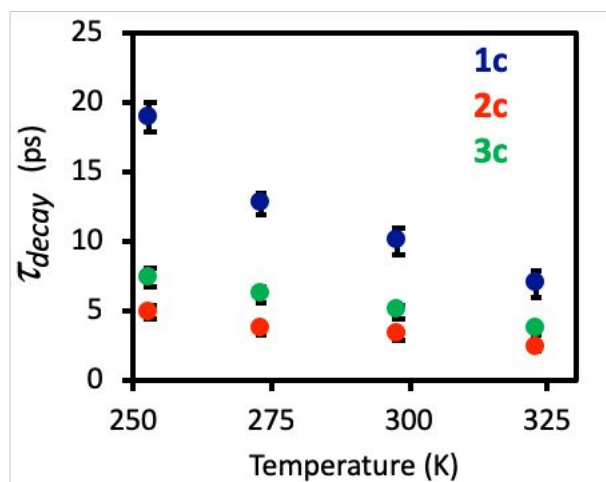


Figure 4. Temperature-dependent excited-state lifetimes of **1c-3c** in acetonitrile performed at temperatures in the range of 253-323 K.

3.2.4 Pendant-group dependence of excited-state dynamics in thienothiophene-core switches (**2c,4c,5c**).

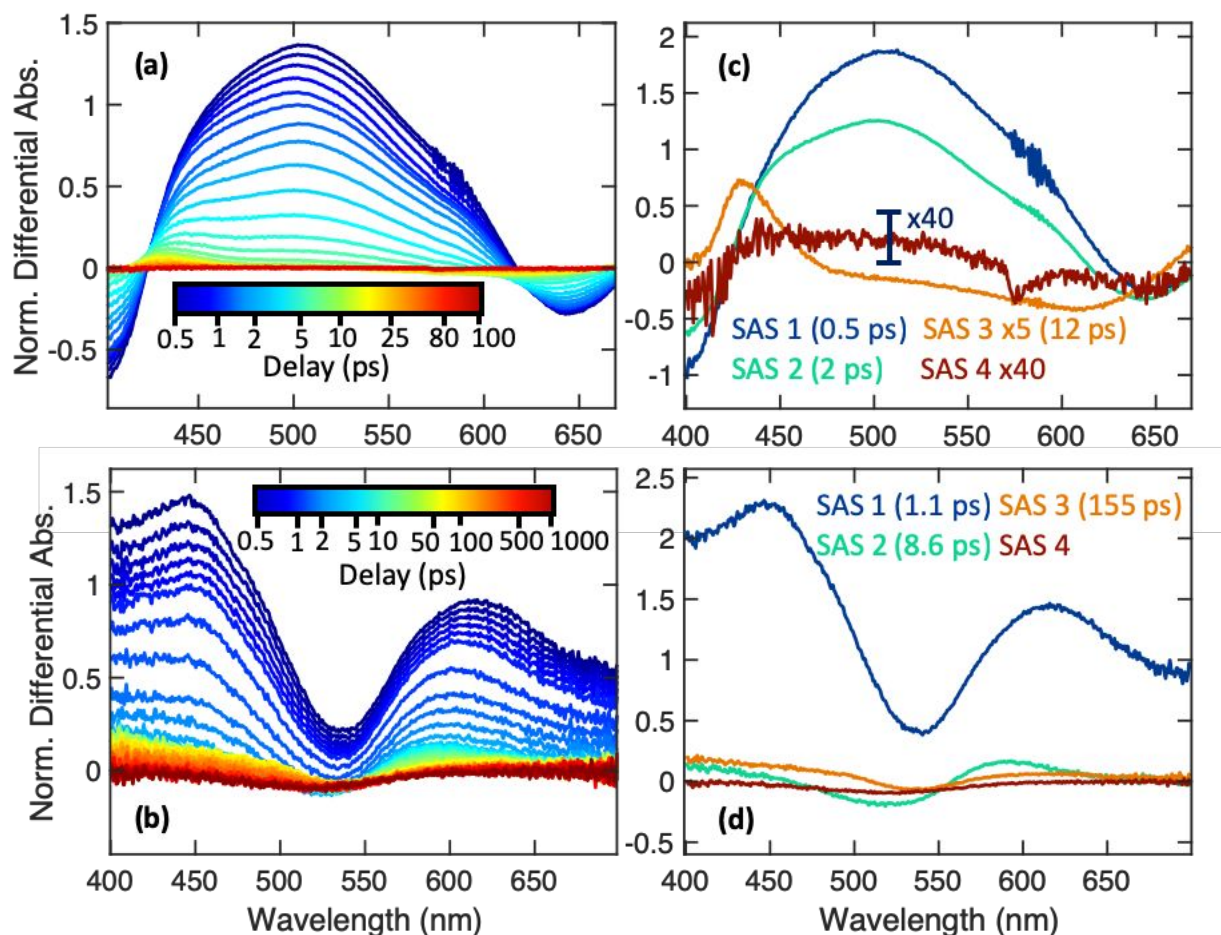


Figure 5. Transient absorption spectra collected for **4c** (a), **5c** (b) in acetonitrile at selected time delays ranging from 0.5 ps to 100 ps (for **4c**) and 1000 ps (for **5c**) as well as the corresponding SAS as determined through global fitting for **4c** (c), and **5c** (d). SAS 3 and 4 in (c) have been scaled as indicated; (c) also includes an error bar (same scale as SAS 4) that represents the S/N level for our measurements). Data was normalized to 1 at maximum absorption at 1 ps.

We also explored the dependence of excited-state dynamics in TT-core switches with variation in pendant group to enable further comparisons with perfluorocyclopentene-core switches. Figure 5a presents the transient spectra for **4c** following excitation at 600 nm. **4c** exhibits a broad excited-state absorption feature spanning the visible with overlapping GSB features at 400 nm and 650 nm. Spectra collected at long pump-probe delays (~ 10 ps) exhibit signatures of a vibrationally hot ground electronic state, as observed for **2c** and **3c**. The spectral data after 0.5 ps was fit to a four-component sequential global fitting model, resulting in timescales associated with

excited-state signal decay 0.5 ps (τ_{decay1}), excited-state decay 2 ps (τ_{decay2}), as well as a vibrational relaxation on the ground state 12 ps ($\tau_{vib.}$). For **4c** the lifetime for SAS 1 needed to be constrained to a minimum of 0.5 ps in order to minimize the residuals and improve the fit quality. Figure 5c shows the SAS for **4c**. SAS 3 and SAS 4 were scaled by factors of 5 and 40, respectively, to highlight spectral shapes more clearly. As with **1c-3c**, we expected to see a permanent bleach signal in SAS 4 reflecting that some cycloreversion occurs. However, due to a very small cycloreversion quantum yield for **4c** (0.44%), the permanent bleach is barely distinguishable from baseline noise, which we estimate is approximately ± 0.005 (normalized differential absorption, relative to maximum absorption at 1 ps) based on baseline fluctuations for signals collected well before time zero. Time dependent cuts taken at representative wavelengths are shown in Figure 6 (column a) at: 405 nm, 440 nm, 530 nm, and 645 nm. Global fits and residuals are presented in Figure S17.

Figure 5b shows the transient spectra of **5c** in acetonitrile following excitation at 530 nm. **5c** exhibits a broad excited state absorption feature encompassing the visible spectrum with an overlapping GSB at 540 nm. The excited state feature appears to decay rapidly leading to a vibrational hot state in the ground electronic state as well as another absorption feature that we attribute to a transient signal from a possible photoproduct. In contrast with **1-4**, this photoswitch was observed to be slightly unstable, forming a permanent photoproduct after prolonged exposure to UV light. Although we were unable to isolate this photoproduct or its steady-state absorption features, TAS signals are largely similar to those measured for other TT switches studied here, indicating that contributing signals arising from the photoproduct are minor at best. As with **1c**, **2c**, and **3c**, **5c** also demonstrates a late time permanent bleach indicative of cycloreversion.

Transient spectra for **5c** were fit with a four-component sequential global fitting model. The SAS for **5c** are shown below in Figure 5d. Time dependent global fits are shown in Figure 6 (column b) at representative wavelengths at 450 nm, 540 nm, 590 nm, and 680 nm, with global fits and residuals presented in Figure S18. The global fits revealed a short-lived electronic excited state (τ_{decay1}) of 1.1 ps and a longer timescale of 8.6 ps associated with vibrational relaxation in the electronic ground state ($\tau_{vib.}$). The global fit also revealed a second long-lived species (SAS3) with a 155 ps lifetime, which may be the result of exciting a photoproduct that also absorbs at 530 nm. The late time spectrum shows permanent bleaching from cycloreversion. The fit results are summarized in Table 2.

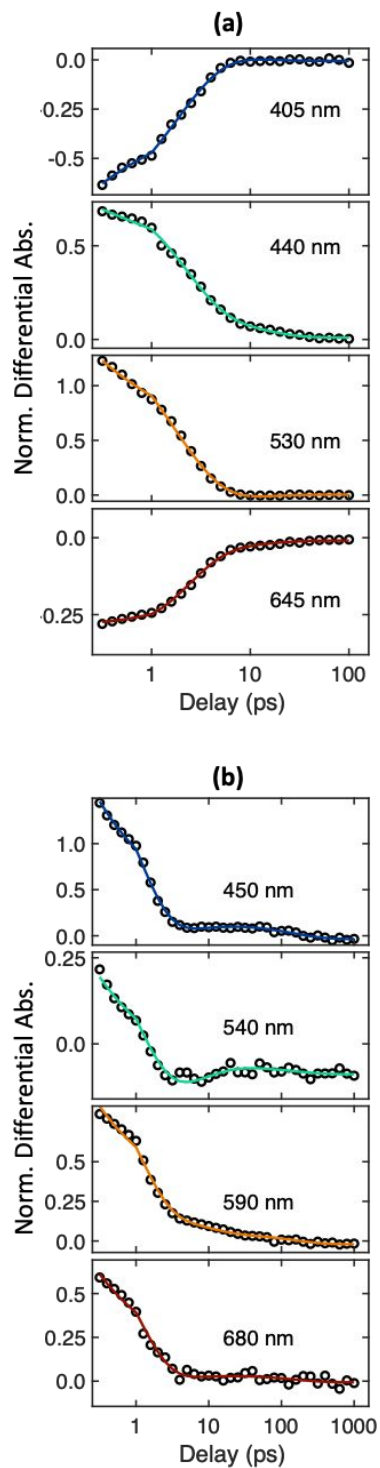


Figure 6. Time-dependent global fits for **4c** (column a) and **5c** (column b) in acetonitrile. Data after 0.5 ps is plotted on a linear scale <1ps and on a logarithmic scale >1ps to clarify early time spectral dynamics.

Table 2. Summary of fit parameters for **4c** and **5c** in acetonitrile.

	τ_{relax} (ps)	$\tau_{decay 1}$ (ps)	$\tau_{decay 2}$ (ps)	$\tau_{vib.}$ (ps)	$\tau_{photoproduct.}$ (ps)
4c	-	0.5	2	12	-
5c	-	1.1	-	8.6	155

3.4 Cycloreversion Quantum yields.

Details of quantum yield determinations are presented in the Supporting Information (e.g. Figures S21-S26). No significant differences in quantum yield for cycloreversion (Φ_{co}) were found for **1-3** after irradiation with 496 nm light at room temperature. All demonstrated relatively high values for Φ_{co} , with Φ_{co} of **1c** (0.32) in close agreement with the values reported by Sumi et al. (~0.297).¹⁴ **5c** also exhibited a modest Φ_{co} of 0.12 following irradiation with 496 nm light. In contrast, the Φ_{co} for **4c** at 590 nm (peak absorption) was drastically lower with a value of only 0.0044. All Φ_{co} results are summarized below in Table 3. Temperature dependent quantum yields were also measured for photoswitches **1-3** at temperatures varying from 253-323K. Results for the temperature dependent quantum yield studies are reported in Figure 7.

Table 3. Summarized Φ_{co} results for **1-5c** at room temperature.

	Φ_{co}
1c	0.32±0.02
2c	0.34±0.03
3c	0.31±0.02
4c	0.0044±0.0003
5c	0.12±0.006

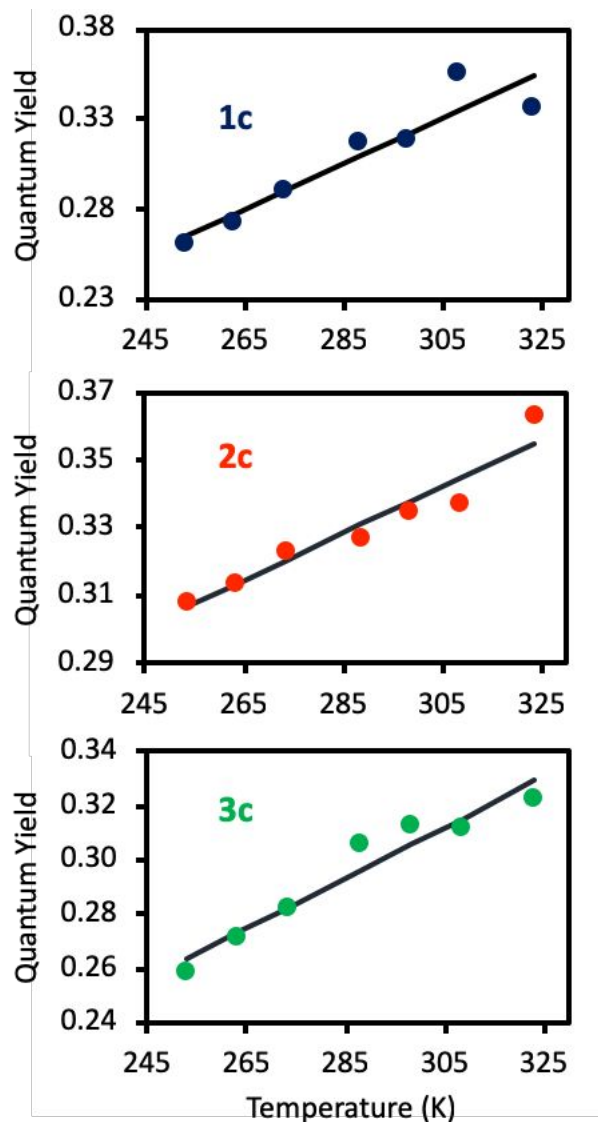


Figure 7. Φ_{co} results for **1-3c** at temperatures ranging from 253-323K in acetonitrile. Each was fit using a linear least squares regression to assist with interpolating the best fit quantum yields for each temperature.

4. Discussion:

The photophysical mechanism for cycloreversion of “normal-type” DAE photoswitches (such as **1c-5c**) can be summarized with the potential energy diagrams sketched in Figure 8^{17, 22, 24, 39}: Photoexcitation occurs to the optically accessible 1^1B state, with rapid crossing to the 2^1A

surface near the Franck-Condon region; the nascent 2^1A population subsequently relaxes towards a local minimum. A barrier associated with lengthening of the reactive C-C bond separates this local minimum (as well as a nonreactive CI with the 1^1A ground-state surface) from the conical intersection through which cycloreversion occurs with branching between both open and cyclized structures. Hence, excited-state deactivation nominally involves parallel nonadiabatic relaxation pathways. Given that a significant fraction of the excited-state population returns to the ground state of the cyclized structure through either pathway, spectroscopic signatures of vibrational cooling should be observed under circumstances of fast electronic deactivation. Below we discuss the behaviors of **1c-5c** and analogous switches within the context of this model.

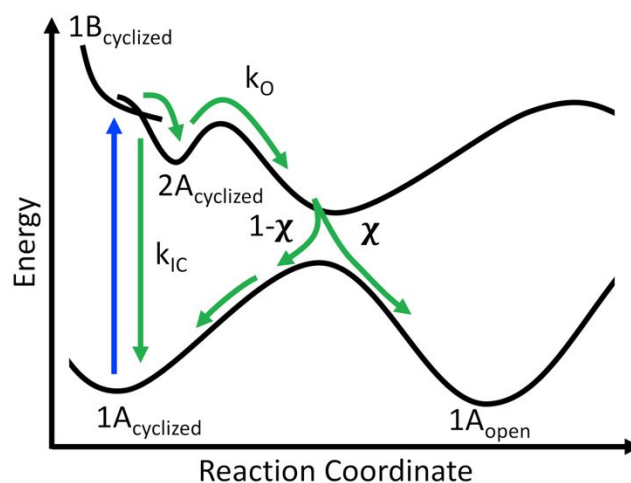


Figure 8. Schematic of potential-energy surfaces and mechanisms for the photoinduced relaxation of **1c-5c**.

4.1 Dependence of deactivation dynamics with core group (in acetonitrile).

Based on results from our transient absorption experiments, the photophysical dynamics of photoswitches **1c-3c** are highly consistent with the picture shown in Figure 8: Each exhibits rapid (sub-picosecond timescales ranging from 0.33-0.5 ps) spectral evolution that likely arise from nuclear relaxation on the 2^1A surface after an ultrafast transit through the 1^1B - 2^1A intersection

near the FC region; this assignment is supported by the fact that only modest changes in SAS features are observed on this timescale from global fits. Based on previous studies, the 1^1B - 2^1A nonadiabatic transition of photoexcited normal-type DAE photoswitches is thought to occur within ~ 100 fs,^{29, 30, 39} a period that would be masked by coherent artifacts in our time-resolved data. Subsequent deactivation from the 2^1A surface occurs on timescales of picoseconds, with lifetimes dependent on the nature of core bridge, pendant groups, temperature, and solvent environment. The reported 2^1A lifetime for **1c** in acetonitrile (at room temperature) is 9.8 ps, which is highly consistent with our observed value of 8.9 ps.⁴⁷ In comparison, the switches with rigid core structures (**2c** and **3c**) deactivate from the 2^1A state on timescales of 2.5 ps and 3.1 ps respectively. Finally, vibrational cooling is observed for **2c-3c**, both of which have rapid excited-state (2^1A) deactivation rates.

Based on our findings with **1c-3c**, structural sensitivity of excited-state dynamics for this series appears to be affected principally by core rigidity rather than aromaticity, as apparent by the similar behavior of **2c** and **3c** and their dissimilar behavior compared to **1c**: specifically, the excited-state lifetimes of the rigid structures are comparable and consistently much shorter than that of **1c** in both high and low polarity solvents (acetonitrile and cyclohexane; dynamics in cyclohexane are discussed in further below). We posit that structural rigidity likely impacts the shapes of the 2^1A potential-energy surface and facilitates rapid dynamics towards conical intersections through which cycloreversion and nonreactive deactivation (“internal conversion”) occurs. Notably, although the rigidity of the core structure impacts the excited-state lifetimes, it does not appear to significantly impact the cycloreversion quantum yield: as shown in Table 3, the cycloreversion quantum yields of **1c-3c** fall within error of each other at room temperature (~ 0.32). This implies that any changes to the potential energy surface and consequently nuclear dynamics that result

from structural modification has a roughly balanced impact on nonreactive and reactive deactivation for this set of switches with benzothiophene pendant groups.

In order to better understand how the core bridging group impacts the shape of the 2^1A potential-energy surface, we conducted a series of temperature-dependent measurements of the cycloreversion quantum yields and 2^1A lifetimes for **1c-3c**, similar in nature to a previous study by Ishibashi et al. for **1c** in n-hexane.³² We used these data to determine the relative rates for cycloreversion and nonreactive deactivation and energy barriers associated with these pathways based on their dependence with temperature. Assuming parallel kinetic deactivation of the 2^1A state, the rates for internal conversion (k_{IC}) and cycloreversion (k_O) can be determined using the total 2^1A decay rate and quantum yield. Similar to Ishibashi et al., we employed two approaches for determining these rates: The first approach assumes that all excited-switches that overcome the barrier to the cycloreversion CI will open. The rates for each process are then determined as

$$k_O(T) = \frac{\phi_O(T)}{\tau_{2A}(T)} \quad (1)$$

$$k_{IC}(T) = \frac{1}{\tau_{2A}(T)} - k_O(T) \quad (2)$$

In the second approach we assumed that only 55% (χ) of the excited-state population that overcomes this barrier will reopen, thereby accounting for branching between the closed and open isomers at the cycloreversion CI. The rates determined by this method are:

$$k_O(T) = \frac{\phi_O(T)}{0.55 * \tau_{2A}(T)} \quad (3)$$

$$k_{IC}(T) = \frac{1}{\tau_{2A}(T)} - k_O(T) \quad (4)$$

We adopted this branching ratio (determined by Ishibashi et al. for **1c**) for all three switches as we do not anticipate significant differences in the shapes of the excited-state potential energy surface for the open structure.³² We find that the rate of internal conversion k_{IC} , is consistently higher than the rate of cycloreversion k_O for all three photoswitches as determined without branching. This can be expected because internal conversion must account for most of the excited-state deactivation with this model. In contrast, when branching is included, k_{IC} is significantly decreased as there are two pathways for deactivation back to the ground state of the cyclized structure.

We used the temperature-dependence of these rates to determine the activation energies, enthalpies, and entropies for the two deactivation pathways according Equations 5 and 6:

$$\ln(k(T)) = \ln(A) - \frac{E_a}{RT} \quad (5)$$

$$\ln(k(T)) - \ln\left(\frac{k_b T}{h}\right) = \frac{-\Delta H^\ddagger}{RT} + \frac{\Delta S^\ddagger}{R} \quad (6)$$

Temperature dependent rates fit to the Arrhenius equation (Equation 5) are plotted in Figure 9; plots fit to Equation 6 are presented in the SI (Figure S27). Thermodynamic activation parameters determined from these fits are summarized in Table 5.

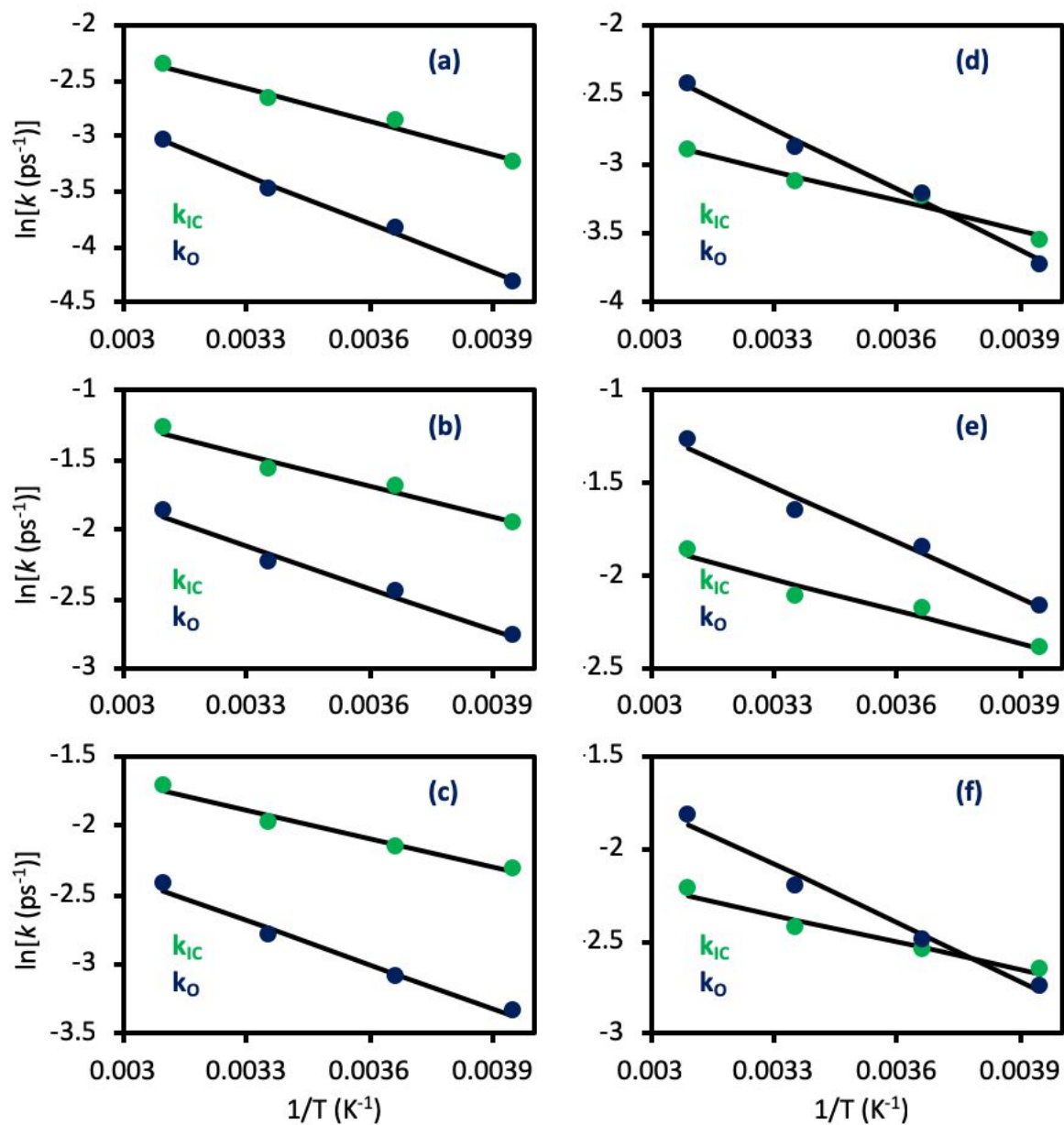


Figure 9 Arrhenius plots for **1c-3c** in acetonitrile without (a-c respectively) and with (d-f respectively) branching between closed and open structures at the cycloreversion CI.

Table 5. Thermodynamic activation parameters for **1c-3c** in acetonitrile.

Species	Without Branching			With Branching		
	E_A kcal/mol	ΔH^\ddagger kcal/mol	ΔS^\ddagger kcal/mol K	E_A kcal/mol	ΔH^\ddagger kcal/mol	ΔS^\ddagger kcal/mol K
1 k_{IC}	2.0	1.4	-0.004	1.4	0.88	-0.007
2 k_{IC}	1.5	0.93	-0.004	1.1	0.58	-0.006
3 k_{IC}	1.4	0.80	-0.005	1.0	0.41	-0.003
1 k_O	2.9	2.3	-0.003	2.9	2.3	-0.0014
2 k_O	2.0	1.4	-0.003	2.0	1.4	-0.0019
3 k_O	2.1	1.5	-0.004	2.1	1.5	-0.003

Our results for **1c** are consistent with those reported previously by Ishibashi et al. Those authors report activation energies for **1c** in n-hexane as 1.3 kcal/mol for IC and 4.2 kcal/mol for cycloreversion when branching at the cycloreversion CI is included.³² While we find a similar value for IC (1.4 kcal/mol), we obtain a barrier for cycloreversion that is more than 1 kcal/mol lower in energy (2.9 kcal/mol). This difference could be the result of solvent stabilization effects on the shape of the 2^1A surface, as the barrier to the cycloreversion CI is associated with an avoided surface crossing; alternatively, this could be associated with differences in solvent-induced barriers for structural reorganization. This difference in activation barrier is consistent with net slower deactivation dynamics in cyclohexane vs. acetonitrile observed here and discussed in detail below.

Based on these analyses, we find that **1c** exhibits higher activation energies and enthalpies for both deactivation pathways than **2c** and **3c** when analyzed with and without branching at the cycloreversion CI. It is most plausible that the inherent flexibility of the perfluorocyclopentene core group allows for structural relaxation to a lower-energy local minimum on the excited-state surface than is accessible to the rigid core photoswitches. In contrast, rigid core structures, like **2c**

and **3c**, have shallower potential-energy minima on the 2^1A surface due to tighter constraints on structural relaxation. Consequently, we would expect activation barriers to both internal conversion and cycloreversion that are comparatively lower for a switch with a rigid compared to flexible core bridge. Importantly, barriers to both internal conversion and cycloreversion are reduced with the rigid vs. flexible core structure, meaning that cycloreversion yields should remain fairly similar (as observed). In all cases the entropies of activation are negative, consistent with reaching a fairly specific excited-state structure (or set of structures) on the 2^1A surface (e.g. transition state or CI) prior to deactivation.

4.2 Dependence of deactivation dynamics with pendent group (TT core switches in acetonitrile).

In contrast, we find that the cycloreversion QY varies considerably with the nature of the pendent groups on the TT core. This variation is similar to what has been reported previously with the perfluorocyclopentene core and that has been ascribed to how the chemical nature of the pendent groups alters the avoided crossing between states of A symmetry that nominally results in the barrier that separates nonreactive from reactive geometries on the 2^1A surface:¹⁷⁻²⁰ specifically, electron-withdrawing pendent groups destabilize the 2^1A surface of the cyclized isomer, lowering the barrier height and increasing the yields for cycloreversion; in contrast, electron-donating pendent groups stabilize the 2^1A state of the cyclized isomer, resulting in a larger barrier and smaller cycloreversion yield. For the set of structures studied here, we find no substantial differences in QY between photoswitches with the same pendent groups but different cores: In addition to the similarities for **1c-3c**, Nakamura reports that the QY for the perfluorocyclopentene-core analog of **5c** is 0.12, which matches the QY we observed for our thienothiophene core photoswitch.¹⁷

We compare the time-resolved spectroscopy of **2c**, **4c** and **5c** to obtain a global picture of the cycloreversion dynamics' dependence on pendent group. All exhibit fast (< 3 ps) excited-state decay in acetonitrile. **2c** undergoes fast relaxation in the 2^1A state on a sub-picosecond timescale followed by excited state decay with a 2.5 ps lifetime. **4c** differs slightly in that it appears to have two excited-state signal decay timescales (sub-ps and 2.0 ps). The sub-ps decay also appears in the recovery of ground-state bleach below 425 nm, implying bimodal excited-state deactivation, although the origin of this behavior is not clear. We are unable to resolve sub-ps spectral dynamics for **5c**, suggesting that relaxation on the 2^1A surface occurs very rapidly and on a timescale that is obscured by coherent artifacts in our measurement. The 2^1A excited state decays on a fast 1.1 ps timescale which is consistent with what we observe for the other rigid core photoswitches.

The differences in QY and lifetimes for TT-core switches with different pendent groups allows us to compare the relative rates for k_O vs k_{IC} at room temperature. For **2c**, which has a relatively high quantum yield, these rates are relatively similar: 0.056 ps^{-1} and 0.044 ps^{-1} respectively. **4c** on the other hand exhibits drastically different rates of 0.004 ps^{-1} for k_O and 0.50 ps^{-1} for k_{IC} . **5c** decays with rates of 0.22 ps^{-1} for k_O and 0.78 ps^{-1} for k_{IC} . While the QYs for cycloreversion follow the prediction with electron donating/withdrawing character of the pendent groups, it is interesting to note that the absolute rates for these processes vary considerably between structures.

4.3 Dependence of deactivation dynamics with solvent environment.

Excited-state lifetimes of cyclized perfluorocyclopentene-core photoswitches in nonpolar solvents (n-hexane or cyclohexane) have been reported to range between 9 and 25 ps depending on the nature of pendent groups: Ward and Elles determined that the excited state of 1,2-bis(2,4-

dimethyl-5-phenyl-3-thienyl)perfluoro-cyclopentene decays on a 9 ps timescale.^{29, 30} Shim et al. and Ishibashi et al. both determined the excited-state lifetimes for **1c** and found that for non-polar solvents the excited state decays on a timescale of approximately 22-25 ps.^{46, 47} We similarly observe a 25 ps timescale in cyclohexane. Sotome et al. observed an excited-state lifetime of 12 ps for bis(2-methyl-5-phenylthiophen-3-yl)perfluorocyclopentene.^{39, 40} Ishibashi et al. reports a lifetime for **1c** in acetonitrile as 9.8 ps⁴⁷, which is a close match for our measurements in which we determined an excited state lifetime of 8.9 ps. We are not aware of any reported lifetimes for related switches in acetonitrile.

Spectral dynamics observed on intermediate timescales (3-4 ps) in nonpolar solution environments, as observed for **1c** in cyclohexane, has been rationalized with more than one interpretation; how they are altered in polar solution environments is not well understood. Relaxation timescales of photoexcited cyclized switches have been assigned to different mechanisms in the literature: Ward and Elles attributed a similar timescale observed in TAS and pump-repump-probe measurements with 1,2-bis(2,4-dimethyl-5-phenyl-3-thienyl)perfluoro-cyclopentene in cyclohexane to the barrier crossing on the way to the CI for cycloreversion; this assignment is predicated on the theoretical expectation that a barrier exists between the 2^1A_C minimum and the $2^1A/1^1A$ CI (the 2^1A_0 region in Figure 8).^{29, 30} These authors noted that the ground state does not recover on the faster (3-ps) timescale for their switch²⁹. If this intermediate timescale is associated with barrier crossing depicted in Figure 8, it would also most likely correspond to the timescale over which nonreactive deactivation occurs. This would imply that all nonreactive deactivation occurs via the region of the cycloreversion CI (i.e. at elongated C-C bond-length).

In contrast, Sotome et al. and Shim et al. attributed this timescale to structural and/or conformational changes, and possibly vibrational cooling, of the closed isomer in the 2^1A state; they assign the longer timescale to excited-state decay through parallel internal conversion and cycloreversion pathways, where the rate of the latter is limited by passage over the aforementioned potential barrier.^{39,40,46} This assignment is most strongly supported by near-IR TA data that shows a weak stimulated emission at ~ 1100 nm that persists for the excited-state lifetime and that must originate from a location on the 2^1A surface removed from the cycloreversion CI as well as the supposition that cycloreversion occurs through the same CI as cyclization, which generally occurs on timescales ranging 100s of fs to a few ps.³⁹ A recent time-resolved stimulated Raman study reported by Mathies revealed signatures of structural dynamics on a timescale of a few picoseconds (faster than excited-state deactivation) that could be consistent with either mechanism.⁵⁶

The observed dilation of the 2^1A excited-state lifetime for TT-core switches in cyclohexane vs. acetonitrile is qualitatively consistent with previous reports of solvent dependence for perfluorocyclopentene-core switches.⁴⁷ Furthermore, our data for **1c-3c** in cyclohexane seem consistent with the picture that an intermediate (few ps or less) timescale is associated with structural or conformation dynamics as well as vibrational cooling in the 2^1A state. We do not observe spectral dynamics on such a timescale for the rigid-core **2c** in cyclohexane, although a second rapid lifetime (~ 1 ps) associated with excited state spectral dynamics is observed for **3c**. It is possible that the short, excited-state decay lifetime associated with **3c** in cyclohexane is in fact rapid structural rearrangement on the excited state, which results in dynamics away from the Franck-Condon region for the excited-state absorption transition that results in loss of excited state signal. Relaxation dynamics on the 2^1A surface involving large-scale structural changes to the core

should be inhibited by structural constraints in **2c** and **3c**, and the overall faster excited-state relaxation for both is qualitatively consistent with this picture.

The relationship between solvent polarity and cycloreversion dynamics remains poorly understood for this class of switch. Based on our comparisons of energy barriers determined with temperature dependent data for **1c** in acetonitrile with those by Ishibashi in n-hexane, it is possible that a strongly polar solvent may stabilize regions of the potential energy surface along the cycloreversion reaction coordinate (but not the IC coordinate). However, the reversion QY is roughly the same in both solvents, implying that this modification does not significantly impact competition between reactive and nonreactive deactivation channels; thus, the modifications to these barriers must be offset by, e.g. solvent dependence of Arrhenius prefactors. Similarly, the lack of observable spectral dynamics associated with excited-state relaxation or vibrational cooling in acetonitrile could mean that the rate of these processes is limited by the absence/presence of energy-accepting solvent responses (i.e. solvation).

We also consider the possibility that some of the observed solvent dependence may be related to differences in solvent viscosity rather than solvent polarity. At our lower temperature limit (253 K), the excited-state lifetimes measured in acetonitrile approach similar lifetimes to what we observe in cyclohexane (Figure 4). Notably, the viscosity of acetonitrile at low temperatures (e.g. 0.83 mPa s at 233 K)⁵⁷ approaches that of cyclohexane at room temperature (0.91 mPa s at 298 K)⁵⁸, suggesting that excited-state deactivation is more strongly controlled by solvent viscosity rather than solvent polarity. However, these similarities are likely coincidental, as excited-state lifetimes reported by Ishibashi for **1c** in n-hexane⁴⁷ (a low viscosity solvent, 0.292 mPa s at 300 K)⁵⁹ are similar to lifetimes we observe in cyclohexane at the same temperature, but should be expected to be more similar to what is observed with room-temperature acetonitrile if

viscosity dominated the solvent dependence of excited-state dynamics. In sum, while it seems very likely that local solvent polarity may fundamentally alter the nonradiative deactivation dynamics, more work is required to understand these different behaviors and their dependence on solvent polarity and viscosity.

5. Conclusion.

The systematic investigation of structural, solvent, and temperature dependence on ultrafast dynamics of DAE derivative photoswitches provides new insight into how core and pendant structural motifs impact cycloreversion rates and quantum yields. Ultrafast transient absorption spectroscopy revealed a distinct trend, with rigid core **2c** and **3c** switches demonstrating faster switching than the analogous flexible perfluorocyclopentene core photoswitch, **1c**. Cycloreversion quantum yields appear unaffected by core group structure as we observed similar cycloreversion quantum yields for **1c-3c**. Our temperature dependent data provides insight into this phenomenon; activation energy and enthalpy barriers are lower (i.e. the excited-state surface is shallower) for rigid relative to flexible core switches for both internal conversion and cycloreversion resulting in no net change in the branching ratio for each pathway. Extension of this study to include **4c** and **5c** illustrates the previously noted dependence of cycloreversion quantum yield on pendant group structure, but with increased excited-state deactivation rates due to impacts of TT-core rigidity. Core- and pendant-dependent trends are observed in both acetonitrile and cyclohexane, although excited-state relaxation and deactivation timescales are longer for each switch in cyclohexane; in combination with results of previous solvent-dependent studies of **1c**, the latter suggests solvent-induced modification to the electronic surfaces. Consistent with previous reports, we attribute spectral dynamics on a ~4 ps timescale observed for

1c in cyclohexane to structural rearrangement on the 2^1A surface; these dynamics are less prominent in rigid-core structures, supporting previous assignments that these arise from nuclear relaxation/reorganization in the 2^1A state.

Conflicts of Interest

There are no conflicts of interest to declare.

Acknowledgements

Photophysical studies and synthesis of **2-5** were supported by NSF-CHE-1607821 (A.E.B & J.D.T). Photophysical studies were also supported in part by a JHU Harry and Cleio Greer Fellowship (C. R. H.). We would also like to acknowledge the kind assistance of Joshua Wilhide and the staff at the Molecular Characterization and Analysis Complex at University of Maryland, Baltimore County.

Supplementary Information. Additional transient absorption spectra, their spectral analyses, and methods for determining molar absorptivities and quantum yields are reported.

References

1. Irie, M.; Fukaminato, T.; Matsuda, K.; Kobatake, S., Photochromism of Diarylethene Molecules and Crystals: Memories, Switches, and Actuators. *Chem. Rev.* **2014**, *114* (24), 12174-12277.
2. Irie, M., Diarylethenes for Memories and Switches. *Chem. Rev.* **2000**, *100* (5), 1685-1716.
3. Chen, Y.; Zeng, D. X.; Fan, M. G., Synthesis and Photochromic Properties of Functional Diarylethene with a 2,5-Dihydrothiophene Bridging Unit. *Org. Lett.* **2003**, *5* (9), 1435-1437.

4. Chen, S.; Li, W.; Zhu, W.-H., Novel Ethene-Bridged Diarylethene Photochromic Systems: Self-Assembly, Photoswitches, and Molecular Logic Gates. In *Photon-Working Switches*, Yokoyama, Y. N., Keitaro, Ed. Springer: Japan, 2017; pp 37-68.
5. Staykov, A.; Yoshizawa, K., Photochemical Reversibility of Ring-Closing and Ring-Opening Reactions in Diarylperfluorocyclopentenes. *J. Phys. Chem. C* **2009**, *113* (9), 3826-3834.
6. Staykov, A.; Areephong, J.; Browne, W. R.; Feringa, B. L.; Yoshizawa, K., Electrochemical and Photochemical Cyclization and Cycloreversion of Diarylethenes and Diarylethene-Capped Sexithiophene Wires. *ACS Nano* **2011**, *5* (2), 1165-1178.
7. Morimoto, M.; Kobatake, S.; Irie, M., Multicolor Photochromism of Two- and Three-Component Diarylethene Crystals. *J. Am. Chem. Soc.* **2003**, *125* (36), 11080-11087.
8. Fukaminato, T.; Hirose, T.; Doi, T.; Hazama, M.; Matsuda, K.; Irie, M., Molecular Design Strategy toward Diarylethenes That Photoswitch with Visible Light. *J. Am. Chem. Soc.* **2014**, *136* (49), 17145-17154.
9. Blegler, D.; Hecht, S., Visible-Light-Activated Molecular Switches. *Angew. Chem. Int. Ed.* **2015**, *54* (39), 11338-11349.
10. Herder, M.; Schmidt, B. M.; Grubert, L.; Patzel, M.; Schwarz, J.; Hecht, S., Improving the Fatigue Resistance of Diarylethene Switches. *J. Am. Chem. Soc.* **2015**, *137* (7), 2738-2747.
11. Zhou, J.; Guo, X.; Katz, H. E.; Bragg, A. E., Molecular Switching via Multiplicity-Exclusive E/Z Photoisomerization Pathways. *J. Am. Chem. Soc.* **2015**, *137* (33), 10841-10850.
12. Young, J. D.; Honick, C. R.; Zhou, J.; Pitts, C. R.; Ghorbani, F.; Peters, G. M.; Lectka, T.; Tovar, J. D.; Bragg, A. E., Energy- and Conformer-Dependent Excited-State Relaxation of an E/Z Photoswitchable Thienyl-Ethene. *Phys. Chem. Chem. Phys.* **2019**, *21* (26), 14440-14452.
13. Aloïse, S.; Sliwa, M.; Pawlowska, Z.; Réhault, J.; Dubois, J.; Poizat, O.; Buntinx, G.; Perrier, A.; Maurel, F.; Yamaguchi, S.; Takeshita, M., Bridged Photochromic Diarylethenes Investigated by Ultrafast Absorption Spectroscopy: Evidence for Two Distinct Photocyclization Pathways. *J. Am. Chem. Soc.* **2010**, *132* (21), 7379-7390.
14. Sumi, T.; Takagi, Y.; Yagi, A.; Morimoto, M.; Irie, M., Photoirradiation wavelength dependence of cycloreversion quantum yields of diarylethenes. *Chem. Commun.* **2014**, *50* (30), 3928-3930.
15. Shizuka, T.; Seiya, K.; Tsuyoshi, K.; Masahiro, I., Extraordinarily High Thermal Stability of the Closed-ring Isomer of 1,2-Bis(5-methyl-2-phenylthiazol-4-yl)perfluorocyclopentene. *Chem. Lett.* **2003**, *32* (10), 892-893.
16. Hanazawa, M.; Sumiya, R.; Horikawa, Y.; Irie, M., Thermally irreversible photochromic systems. Reversible photocyclization of 1,2-bis (2-methylbenzo[b]thiophen-3-yl)perfluorocycloalkene derivatives. *J. Chem. Soc., Chem. Commun.* **1992**, (3), 206-207.
17. Nakamura, S.; Uchida, K.; Hatakeyama, M., Potential energy surfaces and quantum yields for photochromic diarylethene reactions. *Molecules* **2013**, *18* (5), 5091-103.
18. Irie, M.; Sakemura, K.; Okinaka, M.; Uchida, K., Photochromism of Dithienylethenes with Electron-Donating Substituents. *J. Org. Chem.* **1995**, *60* (25), 8305-8309.
19. Morimitsu, K.; Kobatake, S.; Irie, M., Control of Cycloreversion Quantum Yields of Diarylethenes by Introduction of Substituents at the Reactive Carbons. *Mole. Cryst. Liq. Cryst.* **2005**, *431* (1), 451-454.

20. Tatsumi, Y.; Kitai, J.-i.; Uchida, W.; Ogata, K.; Nakamura, S.; Uchida, K., Photochromism of 1,2-Bis(2-thienyl)perfluorocyclopentene Derivatives: Substituent Effect on the Reactive Carbon Atoms. *J. Phys. Chem. A* **2012**, *116* (45), 10973-10979.
21. Pariani, G.; Quintavalla, M.; Colella, L.; Oggioni, L.; Castagna, R.; Ortica, F.; Bertarelli, C.; Bianco, A., New Insight into the Fatigue Resistance of Photochromic 1,2-Diarylethenes. *J. Phys. Chem. C* **2017**, *121* (42), 23592-23598.
22. Nakamura, S.; Kobayashi, T.; Takata, A.; Uchida, K.; Asano, Y.; Murakami, A.; Goldberg, A.; Guillaumont, D.; Yokojima, S.; Kobatake, S.; Irie, M., Quantum yields and potential energy surfaces: a theoretical study. *J. Phys. Org. Chem.* **2007**, *20* (11), 821-829.
23. Rode, M. F.; Sobolewski, A. L., Effect of Chemical Substituents on the Energetical Landscape of a Molecular Photoswitch: An Ab Initio Study. *J. Phys. Chem. A* **2010**, *114* (44), 11879-11889.
24. Asano, Y.; Murakami, A.; Kobayashi, T.; Goldberg, A.; Guillaumont, D.; Yabushita, S.; Irie, M.; Nakamura, S., Theoretical Study on the Photochromic Cycloreversion Reactions of Dithienylethenes; on the Role of the Conical Intersections. *J. Am. Chem. Soc.* **2004**, *126* (38), 12112-12120.
25. Boggio-Pasqua, M.; Ravaglia, M.; Bearpark, M. J.; Garavelli, M.; Robb, M. A., Can Diarylethene Photochromism Be Explained by a Reaction Path Alone? A CASSCF Study with Model MMVB Dynamics. *J. Phys. Chem. A* **2003**, *107* (50), 11139-11152.
26. Perrier, A.; Aloise, S.; Olivucci, M.; Jacquemin, D., Inverse versus Normal Dithienylethenes: Computational Investigation of the Photocyclization Reaction. *J. Phys. Chem. Lett.* **2013**, *4* (13), 2190-2196.
27. Ishibashi, Y.; Fujiwara, M.; Umesato, T.; Saito, H.; Kobatake, S.; Irie, M.; Miyasaka, H., Cyclization Reaction Dynamics of a Photochromic Diarylethene Derivative as Revealed by Femtosecond to Microsecond Time-Resolved Spectroscopy. *J. Phys. Chem. C* **2011**, *115* (10), 4265-4272.
28. Tamai, N.; Saika, T.; Shimidzu, T.; Irie, M., Femtosecond Dynamics of a Thiophene Oligomer with a Photoswitch by Transient Absorption Spectroscopy. *J. Phys. Chem.* **1996**, *100* (12), 4689-4692.
29. Ward, C. L.; Elles, C. G., Controlling the Excited-State Reaction Dynamics of a Photochromic Molecular Switch with Sequential Two-Photon Excitation. *J. Phys. Chem. Lett.* **2012**, *3* (20), 2995-3000.
30. Ward, C. L.; Elles, C. G., Cycloreversion Dynamics of a Photochromic Molecular Switch via One-Photon and Sequential Two-Photon Excitation. *J. Phys. Chem. A* **2014**, *118* (43), 10011-10019.
31. Jean-Ruel, H.; Cooney, R. R.; Gao, M.; Lu, C.; Kochman, M. A.; Morrison, C. A.; Miller, R. J. D., Femtosecond Dynamics of the Ring Closing Process of Diarylethene: A Case Study of Electrocyclic Reactions in Photochromic Single Crystals. *J. Phys. Chem. A* **2011**, *115* (45), 13158-13168.
32. Ishibashi, Y.; Umesato, T.; Kobatake, S.; Irie, M.; Miyasaka, H., Femtosecond Laser Photolysis Studies on Temperature Dependence of Cyclization and Cycloreversion Reactions of a Photochromic Diarylethene Derivative. *J. Phys. Chem. C* **2012**, *116* (7), 4862-4869.

33. Ern, J.; Bens, A.; Martin, H. D.; Mukamel, S.; Schmid, D.; Tretiak, S.; Tsiper, E.; Kryschi, C., Femtosecond reaction dynamics of a photochromic dithienylethene derivative. *J. Lumin.* **2000**, *87-89*, 742-744.
34. Tamai, N.; Miyasaka, H., Ultrafast Dynamics of Photochromic Systems. *Chem. Rev.* **2000**, *100* (5), 1875-1890.
35. Arruda, B. C.; Sension, R. J., Ultrafast polyene dynamics: the ring opening of 1,3-cyclohexadiene derivatives. *Phys. Chem. Chem. Phys.* **2014**, *16* (10), 4439-4455.
36. Shibata, K.; Muto, K.; Kobatake, S.; Irie, M., Photocyclization/Cycloreversion Quantum Yields of Diarylethenes in Single Crystals. *J. Phys. Chem. A* **2002**, *106* (1), 209-214.
37. Fukaminato, T.; Umemoto, T.; Iwata, Y.; Yokojima, S.; Yoneyama, M.; Nakamura, S.; Irie, M., Photochromism of Diarylethene Single Molecules in Polymer Matrices. *J. Am. Chem. Soc.* **2007**, *129* (18), 5932-5938.
38. Kobatake, S.; Yamada, T.; Uchida, K.; Kato, N.; Irie, M., Photochromism of 1,2-Bis(2,5-dimethyl-3-thienyl)perfluoro-cyclopentene in a Single Crystalline Phase. *J. Am. Chem. Soc.* **1999**, *121* (11), 2380-2386.
39. Sotome, H.; Nagasaka, T.; Une, K.; Morikawa, S.; Katayama, T.; Kobatake, S.; Irie, M.; Miyasaka, H., Cycloreversion Reaction of a Diarylethene Derivative at Higher Excited States Attained by Two-Color, Two-Photon Femtosecond Pulsed Excitation. *J. Am. Chem. Soc.* **2017**, *139* (47), 17159-17167.
40. Sotome, H.; Nagasaka, T.; Une, K.; Okui, C.; Ishibashi, Y.; Kamada, K.; Kobatake, S.; Irie, M.; Miyasaka, H., Efficient Cycloreversion Reaction of a Diarylethene Derivative in Higher Excited States Attained by Off-Resonant Simultaneous Two-Photon Absorption. *J. Phys. Chem. Lett.* **2017**, *8* (14), 3272-3276.
41. Murakami, M.; Miyasaka, H.; Okada, T.; Kobatake, S.; Irie, M., Dynamics and mechanisms of the multiphoton gated photochromic reaction of diarylethene derivatives. *J. Am. Chem. Soc.* **2004**, *126* (45), 14764-72.
42. Luchita, G.; Bondar, M. V.; Yao, S.; Mikhailov, I. A.; Yanez, C. O.; Przhonska, O. V.; Masunov, A. E.; Belfield, K. D., Efficient Photochromic Transformation of a New Fluorenyl Diarylethene: One- and Two-Photon Absorption Spectroscopy. *ACS Appl. Mater. Interfaces* **2011**, *3* (9), 3559-3567.
43. Ern, J.; Bens, A. T.; Martin, H. D.; Mukamel, S.; Tretiak, S.; Tsyganenko, K.; Kuldova, K.; Trommsdorff, H. P.; Kryschi, C., Reaction Dynamics of a Photochromic Fluorescing Dithienylethene. *J. Phys. Chem. A* **2001**, *105* (10), 1741-1749.
44. Ern, J.; Bens, A. T.; Martin, H. D.; Mukamel, S.; Schmid, D.; Tretiak, S.; Tsiper, E.; Kryschi, C., Reaction dynamics of photochromic dithienylethene derivatives. *Chem. Phys.* **1999**, *246* (1), 115-125.
45. Tani, K.; Ishibashi, Y.; Miyasaka, H.; Kobatake, S.; Irie, M., Dynamics of Cyclization, Cycloreversion, and Multiphoton-Gated Reaction of a Photochromic Diarylethene Derivative in Crystalline Phase. *J. Phys. Chem. C* **2008**, *112* (30), 11150-11157.
46. Shim, S.; Joo, T.; Bae, S. C.; Kim, K. S.; Kim, E., Ring Opening Dynamics of a Photochromic Diarylethene Derivative in Solution. *J. Phys. Chem. A* **2003**, *107* (40), 8106-8110.
47. Ishibashi, Y.; Umesato, T.; Fujiwara, M.; Une, K.; Yoneda, Y.; Sotome, H.; Katayama, T.; Kobatake, S.; Asahi, T.; Irie, M.; Miyasaka, H., Solvent Polarity Dependence of

Photochromic Reactions of a Diarylethene Derivative As Revealed by Steady-State and Transient Spectroscopies. *J. Phys. Chem. C* **2016**, *120* (2), 1170-1177.

48. Peters, G. M.; Tovar, J. D., Pendant Photochromic Conjugated Polymers Incorporating a Highly Functionalizable Thieno[3,4-b]thiophene Switching Motif. *J. Am. Chem. Soc.* **2019**, *141* (7), 3146-3152.

49. Skov, A. B.; Ree, N.; Gertsen, A. S.; Chabera, P.; Uhlig, J.; Lissau, J. S.; Nucci, L.; Pullerits, T.; Mikkelsen, K. V.; Nielsen, M. B.; Sølling, T. I.; Hansen, T., Excited-State Topology Modifications of the Dihydroazulene Photoswitch Through Aromaticity. *ChemPhotoChem* **2019**, *3* (8), 619-629.

50. Smith, M. C.; Snyder, J. A.; Streifel, B. C.; Bragg, A. E., Ultrafast Excited-State Dynamics of ortho-Terphenyl and 1,2-Diphenylcyclohexene: The Role of "Ethylenic Twisting" in the Nonadiabatic Photocyclization of Stilbene Analogs. *J. Phys. Chem. Lett.* **2013**, *4* (11), 1895-1900.

51. Fleming, C.; Remón, P.; Li, S.; Simeth, N. A.; König, B.; Grøtli, M.; Andréasson, J., On the use of diarylmaleimide derivatives in biological contexts: An investigation of the photochromic properties in aqueous solution. *Dyes Pigments* **2017**, *137*, 410-420.

52. Yu, W.; Magnanelli, T. J.; Zhou, J.; Bragg, A. E., Structural Heterogeneity in the Localized Excited States of Poly(3-hexylthiophene). *J. Phys. Chem. B* **2016**, *120* (22), 5093-5102.

53. Molloy, M. S.; Snyder, J. A.; Bragg, A. E., Structural and Solvent Control of Nonadiabatic Photochemical Bond Formation: Photocyclization of o-Terphenyl in Solution. *J. Phys. Chem. A* **2014**, *118* (22), 3913-3925.

54. Stranius, K.; Börjesson, K., Determining the Photoisomerization Quantum Yield of Photoswitchable Molecules in Solution and in the Solid State. *Sci. Rep.* **2017**, *7*, 41145.

55. Roibu, A.; Fransen, S.; Leblebici, M. E.; Meir, G.; Van Gerven, T.; Kuhn, S., An accessible visible-light actinometer for the determination of photon flux and optical pathlength in flow photo microreactors. *Sci. Rep.* **2018**, *8* (1), 5421.

56. Valley, D. T.; Hoffman, D. P.; Mathies, R. A., Reactive and unreactive pathways in a photochemical ring opening reaction from 2D femtosecond stimulated Raman. *Phys. Chem. Chem. Phys.* **2015**, *17* (14), 9231-9240.

57. Pugachev, Y. F., Absonderung der reinigen Acetonitril und gamma-Butyrlakton nach Zonenschmelzemethode und Untersuchung der Temperaturabhängigkeit von Viskositätskoeffizienten. *Izv. Vyssh. Uchebn. Zaved. Khim. Khim. Tekhnol.* **1991**, *34*, 111-113.

58. Dean, J. A., *Lange's Handbook of Chemistry*. 15th ed.; McGraw-Hill: New York, NY, 1998; p 1424.

59. Michailidou, E. K.; Assael, M. J.; Huber, M. L.; Perkins, R. A., Reference Correlation of the Viscosity of n-Hexane from the Triple Point to 600 K and up to 100 MPa. *J. Phys. Chem. Ref. Data* **2013**, *42* (3), 033104.

TOC Graphic:

